

TL-CLIP: A Power-specific Multimodal Pre-trained Visual Foundation Model for Transmission Line Defect Recognition

Ke Zhang, *Member, IEEE*, Zhaoye Zheng, Yurong Guo, Jiacun Wang, *Senior Member, IEEE*, Jiyuan Yang, and Yangjie Xiao

Abstract—Transmission line defect recognition models have traditionally used general pre-trained weights as the initial basis for their training. These models often suffer weak generalization capability due to the lack of domain knowledge in the pre-training dataset. To address this issue, we propose a two-stage transmission-line-oriented contrastive language-image pre-training (TL-CLIP) framework, which lays a more effective foundation for transmission line defect recognition. The pre-training process employs a novel power-specific multimodal algorithm assisted with two power-specific pre-training tasks for better modeling the power-related semantic knowledge contained in the inspection data. To fine-tune the pre-trained model, we develop a transfer learning strategy, namely fine-tuning with pre-training objective (FTP), to alleviate the overfitting problem caused by limited inspection data. Experimental results demonstrate that the proposed method significantly improves the performance of transmission line defect recognition in both classification and detection tasks, indicating clear advantages over traditional pre-trained models in the scene of transmission line inspection.

Index Terms—Transmission lines, defect recognition, vision-language pre-training, visual foundation model, transfer learning.

I. INTRODUCTION

WITH the rapid development of power system construction, transmission line lengths are expanding at an unprecedented rate. As a result, the traditional manual inspection methods no longer meet the growing demands for transmission line inspections. As a result, unmanned aerial vehicle (UAV) inspection technologies, supported by advances in UAV control systems [1], [2], have been widely adopted [3], [4]. Deep-learning-based computer vision (CV) models are employed to intelligently analyze transmission line images captured by UAVs, greatly enhancing the efficiency and quality of inspections [5], [6]. In practical applications of the power industry, the visual foundation model (VFM) is generally used as the training starting point for these power-specific CV

Research supported by the National Natural Science Foundation of China (NSFC) under grant numbers 62076093, 61871182, 62206095, by the Fundamental Research Funds for the Central Universities under grant numbers 2022MS078, 2023JG002, 2023JC006.

K. Zhang, Z. Zheng, Y. Guo, J. Yang and Y. Xiao are with the Department of Electronic and Communication Engineering, North China Electric Power University, Hebei, 071003, P. R. China. K. Zhang is also with Hebei Key Laboratory of Power Internet of Things Technology, North China Electric Power University, Baoding 071003, Hebei, China. K. Zhang is the corresponding author (e-mail: zhangkeit@ncepu.edu.cn).

J. Wang is with the Computer Science and Software Engineering Department, Monmouth University, West Long Branch 07764, USA. (e-mail: jwang@monmouth.edu).

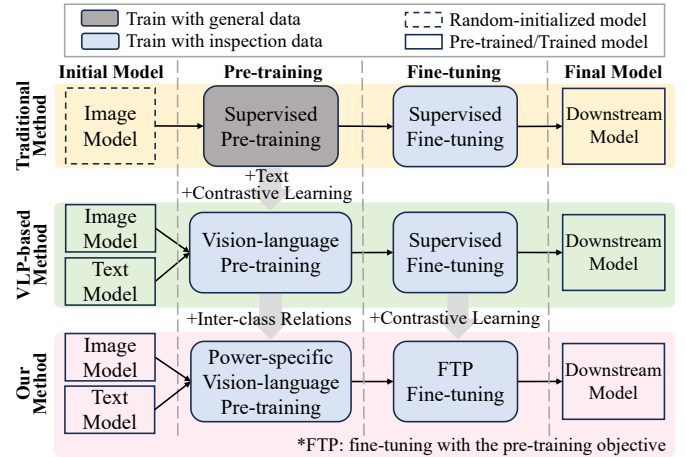


Fig. 1. Training pipelines of different methods for developing transmission line defect recognition models.

models to improve training efficiency [7]–[9]. The VFM is a fundamental model pre-trained on a large-scale dataset that can be adapted to various of downstream tasks [10].

Due to the domain gap between transmission line inspection images and general images, classical VFMs designed for the general domain tasks often perform poorly when directly used for power domain tasks [11]–[13]. Various customized improvements have been proposed, including modifications to model architectures [14], [15] and training strategies [16], [17] for better capturing power-related semantic knowledge. However, none of these works improve the model from the initial training phase that has a crucial impact on the performance of the final model [18]. They typically fine-tune the VFMs obtained from supervised pre-training on general datasets involving everyday objects, *e.g.*, learning image classification on the ImageNet [19], as shown in the yellow box in Fig. 1. Therefore, such VFMs are not built up with power-specific semantics and lack the generalization capabilities necessary for effective defect recognition in transmission line inspections.

Since contrastive language-image pre-training (CLIP) [20] proved the feasibility of learning VFMs with strong transferability through natural language supervision, numerous works about VFMs based on vision-language pre-training (VLP) have emerged [21]–[23]. Pre-training on web-scale image-text data exposes the VFMs to extremely abundant concepts and enables them to acquire rich general semantic knowledge.

Therefore, VLP-based VFMs can provide a starting point with stronger generalization capabilities for fine-tuning or zero-shot testing in downstream tasks than traditional VFMs based on supervised pre-training. More recently, a series of studies have incorporated industry-related knowledge into VLP algorithms to construct domain-specific VFM [24]–[26]. However, no VLP-based VFM has been designed for the power domain. This motivates us to train a professional VFM for transmission line inspection via VLP, which contains abundant power-related semantic knowledge to provide a better training starting point for downstream defect recognition tasks.

Due to the scarcity of the inspection data, training a VLP-based power-specific VFM from scratch is impractical. Therefore, we train the power-specific VFM by adapting an off-the-shelf VLP-based VFM, *i.e.*, Chinese CLIP (CN-CLIP) [21], to the power domain and following the traditional pre-training and fine-tuning pipeline commonly used in the power domain. Here, we first tried a naive VLP-based method to integrate CN-CLIP and the VLP algorithm into the traditional pipeline by introducing additional textual training data and the corresponding pre-training task, namely image-text contrastive learning (ITC), as shown in the green box in Fig. 1. However, we have noticed two key problems in the aforementioned VLP-based pipeline. 1) *Ignored inter-class relations*: Since the pre-training task of CN-CLIP, *i.e.*, ITC, is designed for the general domain, it completely ignores the more complex inter-class relations hidden in the inspection images which results in insufficient learning of power-related semantic knowledge, as shown in Fig. 2(a). 2) *Exacerbated overfitting*: Once we transfer the pre-trained VFM to downstream tasks by supervised fine-tuning, we observe that the overfitting problem caused by limited pre-training data is further exacerbated, as indicated by the dotted lines in Fig. 2(b).

Therefore, in this paper, we focus on modeling power-related semantic knowledge hidden in the unique inter-class relations inside inspection images via VLP, as well as alleviating the overfitting problem in the fine-tuning stage with a dedicated strategy. Specifically, we propose the TL-CLIP framework which has a two-stage training pipeline for pre-training and transferring a power-specific VFM as shown in the red box in Fig. 1. The first stage involves power-specific VLP, where we introduce two novel pre-training tasks designed to model power-related semantic knowledge in potential inter-class relations. Among them, component type matching (CTM) helps to better discriminate the semantics of different types of components while defect-normality comparison (DNC) makes the VFM better understand the abstract concepts of defect and normality. The second stage involves fine-tuning with the pre-training objective where we introduce a novel transfer learning strategy named FTP. It incorporates an additional contrastive learning objective into the fine-tuning stage to alleviate the overfitting problem. With the proposed method, the downstream defect recognition accuracy is further improved and the overfitting problem is also suppressed, as indicated by the solid lines in Fig. 2(b).

It is worth noting that our method improves performance in the power domain through dedicated power-specific training strategies without changing the original model structure,

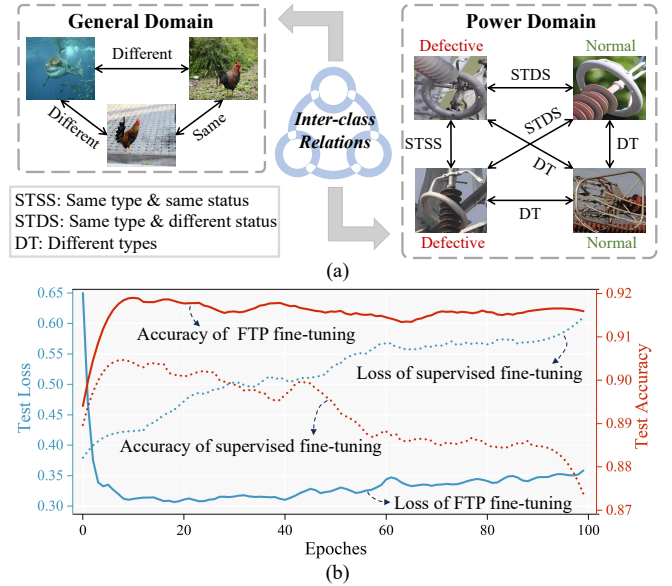


Fig. 2. Two key problems in pre-training and fine-tuning a VLP-based power-specific VFM. (a) The existing pre-training task of the general VLP algorithm ignores the power-specific inter-class relations. (b) The fine-tuning stage of the pre-trained VFM suffers an exacerbated overfitting problem.

thus avoiding the increase in the number of parameters and computational complexity. Therefore, our method is simpler and more efficient than traditional methods. Our main contributions can be summarized as follows:

- 1) We propose a VLP algorithm for pre-training a power-specific VFM, in which the model is pre-trained with ITC and two additional pre-training tasks designed by considering the inter-class relations of instances in inspection images.
- 2) We develop a fine-tuning strategy for better transferring the pre-trained power-specific VFM which uses an additional contrastive learning objective during the fine-tuning stage.
- 3) Extensive experiments demonstrate that the proposed model can effectively improve the accuracy of transmission line defect classification and detection, which indicates that it provides a better foundation for visual recognition tasks in transmission line inspection.

The rest of this article is organized as follows. Section II introduces related works in the area of transmission line defect recognition and VLP-based VFMs. Section III describes how we pre-train our model and transfer it to downstream recognition tasks. Section IV demonstrates the experimental results to verify the effectiveness of our method. Finally, Section V concludes this work and prospects our future work. To enhance readability, Table I lists the key notations utilized throughout this article.

II. RELATED WORKS

A. Transmission Line Defect Recognition

In order to bridge the gap between the general domain and the power domain, the latest research on transmission line defect recognition generally improves the general CV

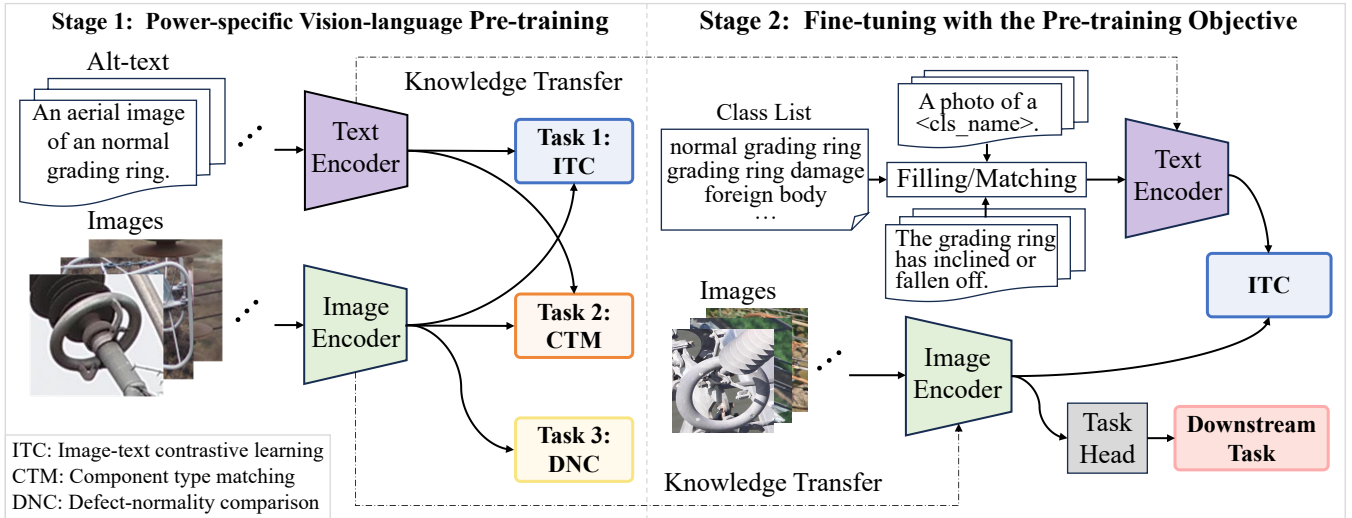


Fig. 3. An overview of the proposed method.

 TABLE I
 MAIN NOTATIONS AND THEIR DEFINITIONS

Notation	Definition
VFM	Visual foundation model
VLP	Vision-language pre-training
ITC	Image-text contrastive learning
CTM	Component type matching
DNC	Defect-normality comparison
FTP	Fine-tuning with the pre-training objective
STSS	Same type and same status
STDS	Same type and different status
DT	Different types
ITTM	Image-text type matching
TITM	Text-image type matching
IITM	Image-image type matching
TTTM	Text-text type matching
GRC	Grading ring comparison
Sup-IN	Supervised pre-training on the ImageNet
n	The batch size
d	The dimension of feature vectors
t	The number of DNC sub-tasks
k	The number of defective grading rings in a batch
q	The number of normal grading rings in a batch
m	The number of grading rings in a batch
τ	The temperature hyper-parameter
ϕ	The function used to judge inter-class relation
σ	The function used to filter specified category
λ_i	The weights of the i -th pre-training loss, $i = 1, 2, 3$
f_i, f_t	The image encoder and text encoder of CN-CLIP
I, T	The input images and alt-texts in a batch
V, L	The image and text feature matrices output by f_i and f_t
v_i, l_i	The i -th feature vector in V and L , $i = 1, 2, \dots, n$
V', L'	The shuffled image and text feature matrices
v'_i, l'_i	The i -th feature vector in V' and L' , $i = 1, 2, \dots, n$
y, y'	The original and shuffled label vectors
W_{ctm}	The mapping matrix used in CTM
P^{ittm}	The prediction matrix of ITTM
Y^{ittm}	The ground truth matrix of ITTM
V^{dgr}	The feature matrix of defective grading rings
V^{ngr}	The feature matrix of normal grading rings
V^{gr}	The feature matrix of all grading rings
S^{gr}	The similarity score matrix of GRC
Z^{gr}	The ground truth matrix of GRC

model from the perspective of model architecture and training strategy based on the characteristics of inspection images.

Researchers often introduce more complex and expressive model architectures, such as attention mechanisms and feature fusion structures, to help the model capture the semantic knowledge contained in inspection images and model power-related semantic knowledge. Bao et al. [27] introduced the end-to-end coordinate attention module to YOLOv5, which enabled the model to focus on the features from key components rather than the complex backgrounds. Guo et al. [28] designed a new feature enhancement mechanism used after the region of interest pooling layer of Faster R-CNN to obtain a more robust representation. Zhang et al. [29] augmented the DETR with a dilated encoder module to provide multi-scale features of transmission line components for better bolt defect detection. Another line of works helps the model better learn the power-related semantic knowledge from the perspective of training data and objectives rather than model architecture. Li et al. [30] incorporated an intersection-over-union-based sampling strategy into Faster R-CNN to alleviate the problem of class imbalance. Zhao et al. [31] applied knowledge distillation algorithms to different types of object detectors to improve the detection accuracy on the limited dataset of hardware defects. Zhang et al. [32] proposed a transmission line bolt defects generation network that generated abundant pseudo bolt images to improve the performance of bolt defect classification.

However, there is little research on exploring the appropriate training starting point, while most previous works ignore the importance of it. The most related work to this paper is [33], the authors introduced self-supervised learning to pre-train an image encoder which then served as the backbone of the defect detector for fine-tuning. Different from [33] which only leveraged vision modality, we explore the denser power-related semantic knowledge in image-text pairs via VLP to find a better and more professional training starting point.

B. Domain-specific VFM Based on VLP

Since CLIP achieved impressive zero-shot performance on ImageNet classification in 2021, a significant number of works

in the general domain have been proposed for visual recognition tasks and vision-language tasks based on VLP-based VFMs [34]–[36]. In these works, VLP-based VFMs provide a better initialization with abundant semantic knowledge for subsequent fine-tuning or zero-shot testing. Motivated by the stronger transferability demonstrated by VLP-based VFMs compared with traditional VFMs based on supervised pre-training, researchers from different domains have tried to construct domain-specific VFMs based on VLP in the past few years. Wang et al. [37] proposed MedCLIP for medical image recognition which eliminates false negatives with medical knowledge. Han et al. [38] designed two novel fashion-specific pre-training tasks and modified the model architecture for tasks of the fashion domain to pre-train a model supporting multiple tasks of the fashion domain. Mo et al. [39] introduced the idea of semi-supervised learning and designed two pseudo-labeling strategies to make the best use of unpaired data in specialized domains, which exceeds CLIP in both zero-shot image classification and image-text retrieval tasks on the remote sensing benchmark. In particular, Jeong et al. [40] first proposed WinCLIP for the domain of industrial manufacturing which supports both anomaly classification and segmentation tasks.

Unfortunately, the power domain still lacks such a dedicated VFM to support different types of defect recognition tasks in transmission line inspection. In this paper, we focus on the unique properties of transmission line inspection images and design a VLP algorithm for the scenario of transmission line inspection to train a power-specific VFM.

III. METHOD

A. Overall Architecture

In this section, we first outline the two-stage training pipeline of TL-CLIP, with the first stage centered on a power-specific VLP and the second stage fine-tuning resulted model with the pre-training objective, as shown in Fig. 3.

In the stage of power-specific VLP, our purpose is to pre-train a VFM that contains rich power-related semantic knowledge. Based on the inter-class relations of instances in inspection images, we propose two innovative power-specific pre-training tasks to address the limitations of image-text contrastive learning within the power domain, so that the model can better learn power-related semantic knowledge, as shown in the left side of Fig. 3. Specifically, we propose component type matching (CTM) to help the model better perceive the relation between different components through matching multimodal component instances, which avoids confusion between similar categories. Moreover, we further propose defect-normality comparison (DNC) which enables the model to better learn the abstract concepts about normality and defect by comparing normal and defective instances. Thanks to the power-specific VLP, the training starting point provided by our pre-trained VFM has significant advantages over the traditional ones and results in better defect recognition performance.

In the stage of fine-tuning with the pre-training objective, we suppress the overfitting problem during fine-tuning for better downstream performance. We assume that the supervised

learning objective in the traditional fine-tuning process will aggravate the overfitting. So we propose the FTP strategy which introduces the ITC task, *i.e.*, the pre-training objective of contrastive learning, into the fine-tuning stage to alleviate this problem, as shown in the right side of Fig. 3. While performing the ITC task, the image encoder of the pre-trained VFM also serves as the backbone of the downstream defect recognition model to learn the downstream task.

B. Stage 1: Power-specific Vision-language Pre-training

In order to achieve efficient power-specific pre-training, we use the existing open-source VLP-based VFM for initialization to fully utilize the rich general knowledge. Here we employ the CN-CLIP [21] as the baseline by default. Based on the CN-CLIP pre-trained in the general domain, we focus on designing power-specific pre-training tasks so that the model can better learn the semantic knowledge specific to the power domain during pre-training. There are three pre-training tasks in our power-specific VLP, among which ITC is the basic task, CTM and DNC are the auxiliary tasks.

1) *Image-text Contrastive Learning*: In order to prevent the original visual representation in the CN-CLIP from being damaged at the power-specific VLP stage, we perform the ITC task which has guided the general VLP of the CN-CLIP as the basic task in the stage of power-specific VLP [21]. Denote a batch of input images and their alt-texts as \mathbf{I} and \mathbf{T} , respectively. Let:

$$\mathbf{V} = f_i(\mathbf{I}) \quad \text{and} \quad \mathbf{L} = f_t(\mathbf{T}), \quad (1)$$

where $f_i(\cdot)$ is the image encoder, $f_t(\cdot)$ is the text encoder, $\mathbf{V} = [\mathbf{v}_1, \mathbf{v}_2, \dots, \mathbf{v}_n]$ is the image feature matrix, $\mathbf{L} = [\mathbf{l}_1, \mathbf{l}_2, \dots, \mathbf{l}_n]$ is the text feature matrix and n is the batch size. $\mathbf{v}_i, \mathbf{l}_i \in R^d$ represent the feature vectors of the i -th image and its alt-text in the batch, and d is the dimension of the feature vectors. Then the contrastive learning loss can be calculated from two directions:

$$L_{itc}^{i \rightarrow t} = -\frac{1}{n} \sum_{i=1}^n \frac{\exp(\mathbf{v}_i \cdot \mathbf{l}_i / \tau)}{\sum_{j=1}^n \exp(\mathbf{v}_i \cdot \mathbf{l}_j / \tau)}, \quad (2)$$

$$L_{itc}^{t \rightarrow i} = -\frac{1}{n} \sum_{i=1}^n \frac{\exp(\mathbf{l}_i \cdot \mathbf{v}_i / \tau)}{\sum_{j=1}^n \exp(\mathbf{l}_i \cdot \mathbf{v}_j / \tau)}, \quad (3)$$

where τ is the temperature hyper-parameter. Finally, the loss of the ITC task can be formulated as:

$$L_{itc} = (L_{itc}^{i \rightarrow t} + L_{itc}^{t \rightarrow i}) / 2. \quad (4)$$

2) *Component Type Matching*: There are three inter-class relations between two instances in the inspection images. a) *Same type & same status (STSS)*: Two instances belong to the same type of components and both of their status are normal or defective, such as the defective grading rings shown in (1) and (2) of Fig. 4. b) *Same type & different status (STDS)*: Two instances belong to the same type of components, but their status are normal and defective, such as the defective and normal grading rings shown in (2) and (3) of Fig. 4. c) *Different types (DT)*: Two instances belong to different types of components, such as the grading ring and shielded ring

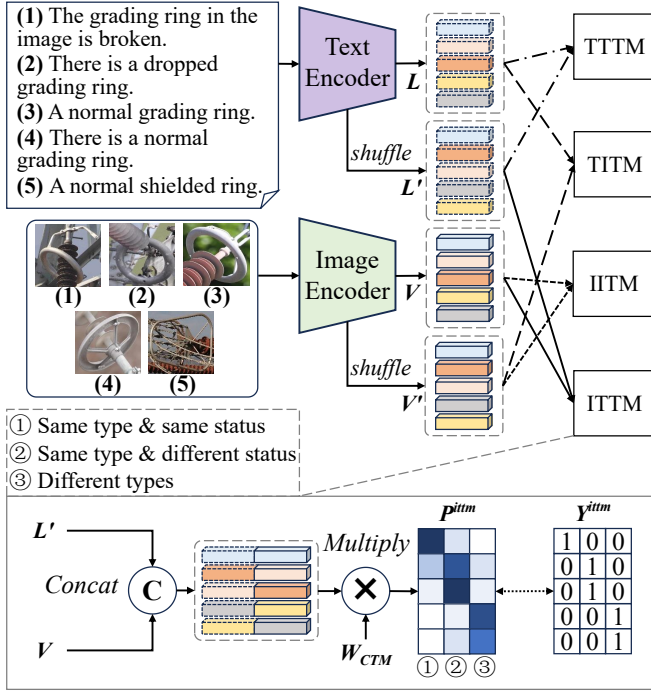


Fig. 4. The implementation of four CTM sub-tasks.

shown in (4) and (5) of Fig. 4. Based on the above widespread relations in inspection images, we design the CTM task to help the model better distinguish different types of components and capture the similarities as well as differences between the same type of components.

In the CTM task, the model is trained to match two randomly paired instances and judge the type of inter-class relation between them. To fully align the semantics between and within modalities, CTM includes four sub-tasks, namely image-text type matching (ITTM), text-image type matching (TITM), image-image type matching (IITM), and text-text type matching (TTTM). Their implementation is shown in Fig. 4.

Taking ITTM as an example, we leverage the aforementioned image feature matrix V and text feature matrix L to implement the sub-task. First, we reorganize the batch of instances to facilitate learning relation judgment by shuffling the order of the feature vectors in L according to a random seed:

$$L' = [l'_1, l'_2, \dots, l'_n], \quad (5)$$

where L' is the text feature matrix with shuffled feature vectors. $l'_i \in R^d$ is the i -th feature vector which may not correspond to the same instance of l_i . As a result, the feature vectors at the same position in V and L' form a random instance pair. Then we use the following formula to model the relations within the random instance pairs of the batch:

$$P^{ittm} = \text{Softmax}(\text{Concat}(V, L') \cdot W_{ctm}), \quad (6)$$

where $\text{Concat}(\cdot, \cdot)$ is a concatenation function that concatenates the corresponding feature vectors in V and L' to obtain a joint feature matrix of shape $n \times 2d$. $W_{ctm} \in R^{2d \times 3}$ is a mapping matrix shared by the four sub-tasks. $P^{ittm} = [p_1^{ittm}, p_2^{ittm}, \dots, p_n^{ittm}]$ is the prediction matrix, in which

$p_i^{ittm} \in R^3$ indicates the probability that the relation between the i -th random instance pair is STSS, STDS, or DT.

On the other hand, to generate the ground truth matrix, we shuffle the original label vector $y = [y_1, y_2, \dots, y_n]$ according to the same random seed used in L' :

$$y' = [y'_1, y'_2, \dots, y'_n], \quad (7)$$

where y' is the shuffled label vector and y'_i is the label corresponding to l'_i . Next, we define function ϕ that judges the inter-class relation between each random instance pair in y and y' :

$$\phi(a, b) = \begin{cases} 1 & \text{if } \langle a, b \rangle \text{ is of STSS} \\ 2 & \text{if } \langle a, b \rangle \text{ is of STDS} \\ 3 & \text{if } \langle a, b \rangle \text{ is of DT} \end{cases}, \quad (8)$$

where $\langle \cdot, \cdot \rangle$ indicates the relation between instances a and b . With the definition of ϕ , we can generate the corresponding label vector in the ground truth matrix Y^{ittm} as follows:

$$y_i^{ittm} = \text{Onehot}(\phi(y_i, y'_i)), \quad (9)$$

where $\text{Onehot}(\cdot)$ is the one-hot encoding function. $y_i^{ittm} \in R^3$ is the i -th label vector in Y^{ittm} which represents the relation of the i -th random instance pair.

Finally, the loss function of the ITTM sub-task can be formulated as:

$$L_{ittm} = -\frac{1}{n} \sum_{i=1}^n \sum_{j=1}^3 y_{ij}^{ittm} \log p_{ij}^{ittm}, \quad (10)$$

where y_{ij}^{ittm} and p_{ij}^{ittm} represent the j -th element in y_i^{ittm} and p_i^{ittm} , respectively.

Similarly, we can also implement the TITM, IITM, and TTTM by reorganizing the instances of the batch in an inter-modal or intra-modal manner, as shown in Fig. 4. The loss of the CTM task can be expressed as:

$$L_{ctm} = (L_{ittm} + L_{titm} + L_{iitm} + L_{tttm}) / 4. \quad (11)$$

where L_{titm} , L_{iitm} , and L_{tttm} are the losses of TITM, IITM, and TTTM respectively.

3) *Defect-normality Comparison*: During training the model with the CTM task, we find that the model is exposed to instances with the DT relation most of the time and has limited opportunities to encounter instances with STSS or STDS relations. This means that the CTM task is still not sufficient to learn the concepts of normality and defect. By observing the data, we note that each component type with both defective and normal status can involve a pair or group of categories. For example, the component type of "grading ring" includes a pair of categories namely "normal grading ring" and "grading ring damage". Based on the observation, we further proposed the DNC task to make the model better understand the abstract concepts of normality and defect.

In the DNC task, we train the model to compare the instances belonging to the same component type and find instances with the same state. We also divide the DNC task into multiple sub-tasks according to the component types with both defective and normal categories in the pre-training dataset, which can be found in Section IV-B.

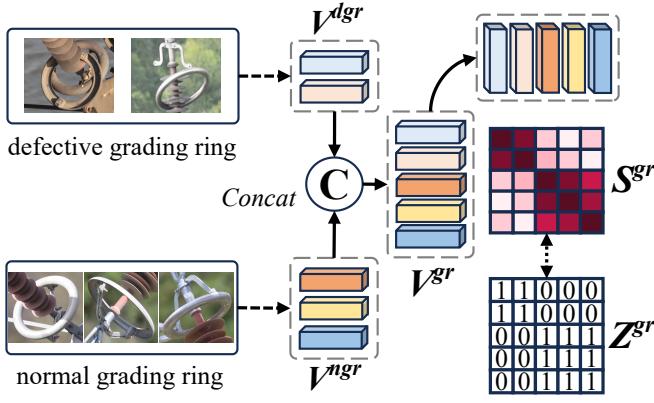


Fig. 5. The implementation of DNC sub-tasks, taking GRC as an example. For the sake of simplicity, we omit the image encoding and filtering process and only highlight the comparison between defective and normal instances.

Taking the component type of grading ring as an example, we denote the corresponding sub-task as grading ring comparison (GRC), the implementation is shown in Fig. 5. First, we need to filter out the feature vectors corresponding to defective and normal grading rings from V , respectively:

$$V^{dgr} = \sigma(V, \mathbf{y}, i_{dgr}) = [v_1^{dgr}, v_2^{dgr}, \dots, v_k^{dgr}], \quad (12)$$

$$V^{ngr} = \sigma(V, \mathbf{y}, i_{ngr}) = [v_1^{ngr}, v_2^{ngr}, \dots, v_q^{ngr}], \quad (13)$$

where $\sigma(\cdot, \cdot, \cdot)$ is a filter function that filters out the feature vectors of the specified category from V according to the label vector \mathbf{y} and the index of the category. i_{dgr} and i_{ngr} represent the category index of defective and normal grading ring. V^{dgr} and V^{ngr} are the image feature matrices consisting of defective and normal feature vectors. v_i^{dgr} and v_j^{ngr} represent the feature vectors of the i -th defective grading ring and j -th normal grading ring. k and q are the number of defective and normal grading rings in the batch.

Then we concatenate V^{dgr} and V^{ngr} to obtain a defect-normality feature matrix of grading rings:

$$V^{gr} = \text{Concat}(V^{dgr}, V^{ngr}), \quad (14)$$

where $V^{gr} \in R^{m \times d}$ is the defect-normality feature matrix of all grading rings in the batch. m is the total number of grading rings in the batch equaling $k + q$. Finally, we calculate the cosine similarity between V^{gr} and its transposed matrix to obtain the similarity score matrix:

$$S^{gr} = \text{Sigmoid}(V^{gr} \cdot (V^{gr})^T) = (s_{ij}^{gr})_{m \times m}, \quad (15)$$

where S^{gr} is the similarity score matrix. s_{ij}^{gr} represents the similarity score between the i -th and j -th grading rings.

Meanwhile, a ground truth matrix for this sub-task is generated according to k and q :

$$Z^{gr} = (z_{ij}^{gr})_{m \times m}, \quad (16)$$

where

$$z_{ij}^{gr} = \begin{cases} 1 & 1 \leq i, j \leq k \text{ or } k < i, j \leq k + q \\ 0 & \text{otherwise} \end{cases}, \quad (17)$$

Then we calculate the loss function of the GRC sub-task as follows:

$$L_{grc} = -\frac{1}{m} \sum_{i=1}^m \sum_{j=1}^m [z_{ij}^{gr} \log s_{ij}^{gr} + (1 - z_{ij}^{gr}) \log (1 - s_{ij}^{gr})], \quad (18)$$

We can also perform sub-tasks corresponding to other component types with similar processes. Finally, the loss of the DNC task can be formulated as

$$L_{dnc} = \frac{1}{t} \sum_{i=1}^t L_{dnc(i)}. \quad (19)$$

where t is the number of the component types with both defective and normal categories, *i.e.*, the number of DNC sub-tasks. $L_{dnc(i)}$ is the loss of i -th DNC sub-task. It is worth noting that the DNC task can be easily extended to other component types by adding only a few lines of code.

When we use the aforementioned three pre-training tasks to pre-train the CN-CLIP, the total loss of the power-specific VLP stage can be formulated as

$$L_{pre-train} = \lambda_1 L_{itc} + \lambda_2 L_{ctm} + \lambda_3 L_{dnc}. \quad (20)$$

where λ_1 , λ_2 and λ_3 are the weights of the three pre-training losses.

C. Stage 2: Fine-tuning with the Pre-training Objective

Since the inspection data that the model can access in the power-specific VLP stage is much smaller than that of the general VLP, the representation of the pre-trained VFM inevitably suffers from an overfitting problem. We find this problem is exacerbated when only the supervised learning objective is used during the fine-tuning stage, leading to inferior fine-tuning results, as shown by the dotted lines in Fig. 2(b). Specifically, the labels used in supervised learning provide stronger supervision signals, leading to more discriminative representations and aggravating overfitting. On the other hand, contrastive learning uses natural language to provide weaker supervision signals, the learned representations will be less discriminative [41]. We verified this quantitatively in our experiments, as can be found in Section IV-E. This inspires us to introduce the ITC task which contains the pre-training objective of contrastive learning into the fine-tuning stage to neutralize the strong discriminative nature of supervised learning for alleviating the overfitting problem, as shown in the right side of Fig. 3.

1) *Transferring to the Defect Classification Task with FTP:* We incorporate the FTP strategy into the fine-tuning stage of the defect classification task from three aspects. Firstly, to address the problem of the classification dataset not containing alt-texts, we randomly use the category name to fill a general template or match a predefined description to generate the alt-text for each image. Secondly, a task head, *i.e.*, classification head, is added to the image encoder of the pre-trained VFM to learn the defect classification task with the traditional

supervised learning objective. The loss of this part can be formulated as:

$$L_{cls} = -\frac{1}{n} \sum_{i=1}^n \sum_{j=1}^c y_{ij}^{cls} \log p_{ij}^{cls}, \quad (21)$$

where c is the number of categories in the dataset. y_{ij}^{cls} and p_{ij}^{cls} represent the label and prediction result of the i -th sample belonging to j -th category. Meanwhile, to introduce contrastive learning into the fine-tuning stage, we retain the text encoder and train it with the image encoder to learn the ITC task. We use Eqs. (2)–(4) to calculate the corresponding loss of ITC. The total loss of the fine-tuning stage can be formulated as:

$$L_{cls-ftp} = L_{cls} + L_{itc}. \quad (22)$$

Finally, we remove the text encoder after the fine-tuning stage and the final classification model consists of the fine-tuned image encoder and the classification head.

2) *Transferring to the Defect Detection Task with FTP*: We further extend the FTP strategy from the defect classification task to the defect detection task from two aspects. Firstly, to enable the model to better perceive the local features for the defect detection task, we crop the bounding boxes in the defect detection dataset at different scales so that the instances in the boxes occupy different proportions. Next, we train the defect detector in two steps. We first train the backbone (*i.e.*, the image encoder of the pre-trained VFM) and the classification branch of the detection head on the multi-scale cropped images with ITC and image classification tasks, in the same way as transferring to the defect classification task. Then we remove the ITC task as well as the text encoder and train the full detector on the original defect detection dataset to learn the location of instances.

Notably, although we use defect classification and detection tasks to verify the performance of our method in this paper, our pre-trained VFM and FTP strategy are not limited to these two tasks. We can also use the pre-trained image encoder of the VFM as the backbone of other defect recognition models and incorporate the FTP strategy into the fine-tuning process of other image-level or region-level downstream tasks in a similar way to the above two cases.

IV. EXPERIMENTS AND ANALYSIS




In this section, we first introduce the datasets used in our experiments and the experimental setup. Then, we compare our method with other existing methods and evaluate the contribution of each innovation through ablation experiments.

A. Datasets

The experimental images used in this paper were obtained by a power inspection department through UAV aerial photography. By annotating and cropping the original inspection images, we constructed three datasets for pre-training our power-specific VFM, evaluating the performance of different models in defect classification and defect detection.

1) *Transmission Line Image-text (TL-it) Dataset*: We use the TL-it dataset to pre-train our power-specific VFM. The

TABLE II
SOME SAMPLES IN THE TL-IT DATASET

Images	Alt-texts	Labels
	There is a normal grading ring in the image.	7
	A rusted shielded ring on the aerial inspection image.	17
	Two shockproof hammers are closely adjacent to each other.	19

TL-it dataset contains 23391 image-text-label triplets covering 24 common categories of normal and defective instances in transmission lines, and some samples from the dataset are shown in Table II. Each image in an image-text-label triplet is obtained by cropping an expert-annotated bounding box from an original transmission line image and each label corresponding to an image is also given by domain experts. In particular, each alt-text in an image-text-label triplet is obtained by filling a general template with the category name corresponding to the label or matching the category name with a predefined description.

2) *Transmission Line Defect Classification (TLDC) Dataset*: We use the TLDC dataset to fine-tune the pre-trained VFM and evaluate its performance in the defect classification task. The TLDC dataset includes 9779 images of 14 types of normal and defective categories in the TL-it dataset. The training set and testing set are divided with a 9:1 ratio.

3) *Transmission Line Defect Detection (TLDD) Dataset*: We use the TLDD dataset to fine-tune the pre-trained VFM and evaluate its performance in the defect detection task. The TLDD dataset includes a total of 1,560 images with 7 defective categories contained in the TL-it dataset as well, in which the the training set and testing set are also divided with a 9:1 ratio.

B. Experimental Settings

We implement the experiments using the PyTorch framework on a workstation with two NVIDIA RTX3090 GPUs. Two types of open-source CN-CLIP models are selected as the baseline, namely CN-CLIP with ResNet50 (RN50) image encoder and CN-CLIP with ViT-B-16 (ViT) image encoder. In the stage of power-specific VLP, we resize the resolution of each input image to 224×224 and both models are pre-trained for 30 epochs with the Adam optimizer. For the CN-CLIP with RN50, the learning rate and the batch size are set to 1×10^{-5} and 335 respectively. For the CN-CLIP with ViT, the learning rate and the batch size are set to 1×10^{-6} and 120 respectively. Because CN-CLIP is based on Chinese, all English texts used in experiments related to the proposed model are translated into Chinese. Since there are six types of components in the TL-it dataset with both defective and normal categories, we divide the DNC task into six sub-tasks.

TABLE III
THE CLASSIFICATION RESULTS ON THE TLDC DATASET

Model	Pre-train	#params/M	Acc/%
RN50	Sup-IN	23.5	87.9
VGG19	Sup-IN	139.6	87.6
EfficientNet	Sup-IN	10.7	86.5
MobileNet v3	Sup-IN	4.2	84.7
ViT	Sup-IN	85.8	83.9
RN50	CLIP	38.3	82.5
ViT	CLIP	86.2	87.7
RN50	CN-CLIP	38.3	88.7
ViT	CN-CLIP	86.2	88.2
RN50	TL-CLIP	38.3	91.6
ViT	TL-CLIP	86.2	93.8

* Bold font represents the first two optimal values.

TABLE IV
THE DETECTION RESULTS ON THE TLDD DATASET

Model	Pre-train	#params/M	mAP/%
Faster RCNN	Sup-IN	41.4	68.8
	CLIP	41.4	72.3
	CN-CLIP	41.4	73.3
	TL-CLIP	41.4	76.4
ViTDet	Sup-IN	115.4	71.6
	CLIP	112.5	75.2
	CN-CLIP	112.5	74.2
	TL-CLIP	112.5	78.1

* Bold font represents the first two optimal values.

Apart from GRC, we denoted other sub-tasks as shielding ring comparison (SRC), shockproof hammer comparison (SHC), bolt comparison (BC), insulator comparison (IC) and foreign-body-like object comparison (FC). In the stage of fine-tuning with the pre-training objective, we replace the backbone of the downstream classification or detection model with the image encoder of the pre-trained VFM and keep the default hyperparameter settings of the original model unchanged.

In defect classification, we use the top-1 accuracy (Acc) to evaluate the performance. In defect detection, we adopt mean average precision (mAP) as the main metric. In particular, average precision (AP) is obtained by calculating the area under the P-R curve of a certain category which represents the detection accuracy of that category and mAP is the mean AP of all categories. Here we adopt 0.5 as the intersection over union (IoU) threshold in computing APs and the corresponding mAP. In addition, we use parameter quantities (#params) to evaluate the model size.

C. Experiments on the TLDC Dataset

We build two classification models based on our pre-trained power-specific VFMs with ViT and RN50 architectures. In order to verify the defect classification performance of our models, we compare a variety of traditional VFMs based on single-modal supervised pre-training on the ImageNet (Sup-IN) and VLP-based VFMs, and the results are shown in Table III. It can be observed that the models with two different architectures based on CN-CLIP have the best performance for defect classification apart from the proposed model, so the

corresponding two open-source CN-CLIP models are selected as the baseline for our study. The two models based on the proposed TL-CLIP achieve the highest Acc of 91.6% and 93.8% respectively, further improving the Acc by 2.9% and 5.6% compared with the ones based on CN-CLIP. The results show that the proposed method has significant advantages over other methods pre-trained on the general domain in the task of transmission line defect classification.

D. Experiments on the TLDD Dataset

In order to verify the effectiveness of the proposed method in defect detection, we replace the RN50 and ViT backbone of Faster R-CNN [42] and ViTDet [43] with the corresponding image encoders of TL-CLIP models respectively. Then we compare the performance of the two detectors with different pre-trained backbones on the TLDD dataset, and the results are shown in Table IV. It can be found that the VLP-based backbone has better performance on the TLDD dataset. The mAP of the detection model based on our TL-CLIP are significantly higher than the ones using traditional Sup-IN and they are improved by 3.1% and 3.9% respectively compared with the baseline of CN-CLIP. It is noteworthy that we only modify the training strategy without introducing new modules into our models, as a result, no new parameters are added to increase the computational burden of the model, as shown in Table III and Table IV.

Fig. 6 shows the detection results of detection models with backbones pre-trained by Sup-IN and our TL-CLIP. As shown in Fig. 6(a) and Fig. 6(d), the detection model based on our TL-CLIP successfully finds the defect of insulator damage in the slightly blurred area while the counterpart based on Sup-IN fails. In Fig. 6(e), the detection model based on our TL-CLIP recognizes the bird nest which is partially obscured by the tower but its counterpart makes a false alarm of foreign body. This also shows that our method can help the model better distinguish semantically similar categories. In Fig. 6(f), the detection model based on our TL-CLIP accurately detects the insulator bunch-drop which only occupies a small proportion of the image. In conclusion, the detection model based on our TL-CLIP performs better than the one based on the traditional Sup-IN when there are blurring, partial obstruction, and small objects in the inspection images.

E. Ablation Analysis

In order to verify the effectiveness of the power-specific VLP algorithm as well as the FTP strategy, we design the ablation experiments to compare and analyze the effect of these improvement schemes.

1) *Ablation Analysis on Power-specific VLP*: Before analyzing the effect of the pre-training task, we first verify the necessity of using the TL-it dataset in the stage of power-specific VLP. Since the power-specific VLP process requires instance-level images, the model can only be pre-trained using the TLDC or TL-it datasets. We use the ITC task to pre-train four VFMs on the two datasets and compare their performance in downstream tasks, as shown in Table V. Regardless of the

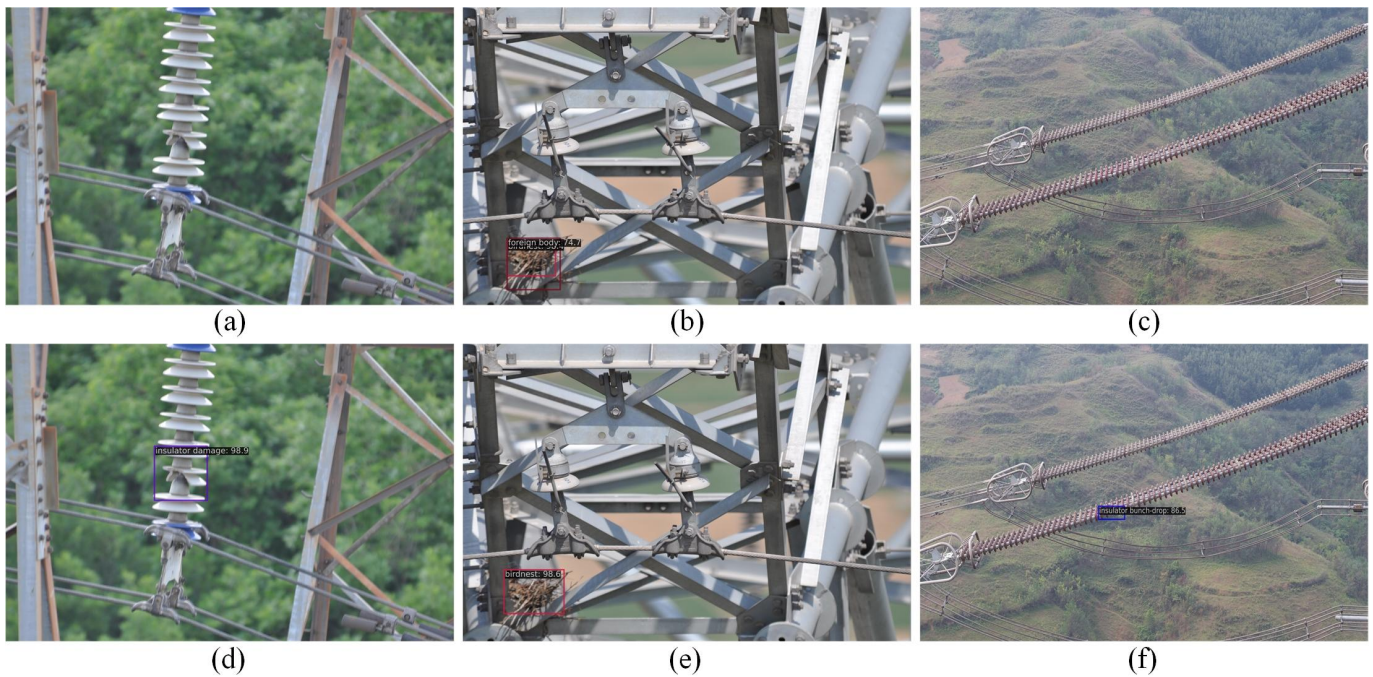


Fig. 6. Detection results of the detection models with different pre-trained backbones. Since the detection results of the two architectures are similar, we only demonstrate the detection results corresponding to the ViT architecture. (a)-(c) ViT pre-trained by Sup-IN. (d)-(f) ViT pre-trained by our TL-CLIP.

TABLE V
EFFECTS OF DIFFERENT PRE-TRAINING DATASETS

Image Encoder	Pre-training Dataset	TLDC	TLDD
		Acc/%	mAP/%
RN50	FDC	88.9	73.3
	FD-it	89.5	73.9
ViT	FDC	89.3	73.0
	FD-it	92.3	75.4

* Bold font represents the optimal value.

TABLE VI
ABLATION ANALYSIS OF PRE-TRAINING TASKS

Image Encoder	ITC	CTM	DNC	TLDC	TLDD
				Acc/%	mAP/%
RN50	-	-	-	88.7	73.3
	✓	-	-	89.5	73.9
	✓	✓	-	90.1	75.4
	✓	-	✓	90.3	75.2
	✓	✓	✓	90.9	75.7
ViT	-	-	-	88.2	74.2
	✓	-	-	92.3	75.4
	✓	✓	-	92.9	75.9
	✓	-	✓	93.1	76.0
	✓	✓	✓	93.3	76.5

* Bold font represents the optimal value.

image encoder architecture used, VFMs pre-trained on the TL-it dataset can achieve better results. This is because the TL-it dataset contains richer visual concepts and more diverse textual data, while the TLCD dataset has fewer categories and can only use category names corresponding to labels as alt-texts for pre-training.

Then we design a set of experiments to evaluate the effect of three pre-training tasks used in the stage of power-specific VLP on defect recognition tasks, the results are shown in Table VI.

It can be seen that using the ITC task to pre-train the VFM with transmission line image-text pairs can effectively improve the Acc and mAP metrics in the downstream defect classification and detection tasks compared with direct fine-tuning the image encoder in an end-to-end (E2E) manner, especially on the ViT architecture. This result verifies the necessity of using the ITC task to adapt CN-CLIP models from the general domain to the power domain. This process can not only help the model incorporate relevant knowledge from transmission line image-text pairs into the existing pre-trained representation but also prevent the pre-trained representation

in CN-CLIP from being destroyed during E2E fine-tuning.

When adding the CTM task on the basis of the ITC task, the Acc and mAP metrics of VFMs with both architectures in downstream defect classification and detection tasks are further improved by 0.5-1.5%. This result shows that introducing the three types of inter-class relations between instances into the pre-training stage can help the model better learn category-related semantic knowledge and distinguish different categories in the transmission line, thereby improving recognition precision. Similarly, the Acc and mAP metrics also increase by 0.6-1.3% when the DNC task is introduced on the basis of the ITC task. The results demonstrate that introducing semantic knowledge contained in the inter-class relations of instances in inspection images into the pre-training process through two novel pre-training tasks can further improve the performance of downstream tasks. In addition, we plot the loss curves of each sub-task of the two designed auxiliary pre-training

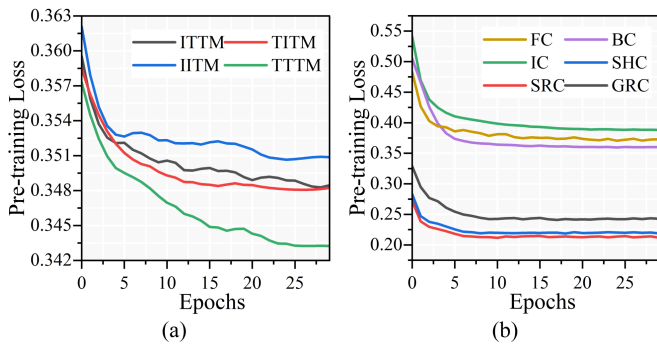


Fig. 7. The loss curves of different sub-tasks. (a) Sub-tasks of CTM. (b) Sub-tasks of DNC.

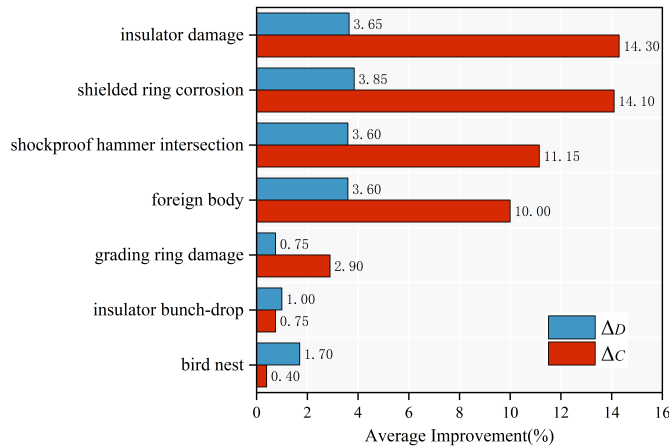


Fig. 8. Improvements in recognition performance of each category before and after the introduction of two auxiliary pre-training tasks, where Δ_C and Δ_D represent the average improvement in defect classification and detection respectively.

tasks during the power-specific VLP stage to verify whether they can be effectively learned by the model, as shown in Fig. 7. It can be seen that all losses can decrease smoothly until convergence, which verifies both tasks can be well learned. As a result, the semantic knowledge contained in the aforementioned inter-class relations is gradually incorporated into the VFM during the pre-training stage.

When we use the three pre-training tasks simultaneously, the Acc corresponding to the two types of image encoders can be improved by 2.2% and 5.1%. The mAP can also be improved by 2.4% and 2.3% respectively. In addition, to verify the promotion effect of the two auxiliary pre-training tasks on various defect recognition, we compared the average improvement of the pre-trained VFM in classification and detection tasks before and after adding the two new pre-training tasks, as shown in Fig. 8. It can be seen that after the introduction of the two novel pre-training tasks, the metrics of both downstream defect recognition tasks for different defects have been improved to varying degrees. This verifies that the two power-specific pre-training tasks we designed can help the model learn power-specific semantic knowledge more fully and effectively.

In order to intuitively observe the impact of power-specific VLP on learning component-related semantics and defect-

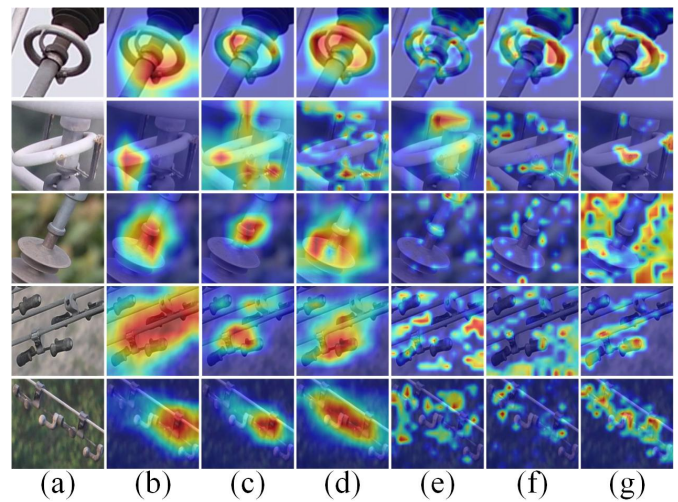


Fig. 9. Instances in inspection images and their corresponding attention maps generated by different models. (a) Original images. (b)-(d) RN50 pre-trained by Sup-IN, CN-CLIP and TL-CLIP. (e)-(g) ViT pre-trained by Sup-IN, CN-CLIP and TL-CLIP.

normality concepts, we visualize the attention maps generated by our VFMs, the baselines and the counterparts based on Sup-IN when reasoning about the instances on inspection images, as shown in Fig. 9. In terms of component-related semantics, we can find from the normal grading ring in the first row and the normal shockproof hammer in the fourth row that both of our models can find the components in the image and focus on the regions with key semantics accurately. However, other models either fail to find the component or cannot focus on the regions with key semantics. This indicates that the power-specific VLP makes our model more sensitive to component-related semantics and can more accurately recognize different component categories. In terms of defect-normality concepts, we can see that our model can effectively focus on the key regions representing defective or normal states from the first three rows and the last two rows. For example, our model accurately finds the dropped grading ring and the breakpoint in the second row. They also find the defect of shockproof hammer intersection by locating the two shockproof hammers and detecting the contact point between them while other models fail, as shown in the fifth row of Fig. 9. This proves that our model has learned the abstract defect-normality concept in the stage of power-specific VLP and can better perceive defects in the instances.

2) *Ablation Analysis on FTP*: Before evaluating the effect of FTP, we first qualitatively verify our hypothesis that supervised learning will exacerbate the overfitting problem during the fine-tuning stage. We use t-SNE [44] to visualize the 7 defect categories in the image feature space fine-tuned with different types of objects, as shown in Fig. 10. As can be seen, CN-CLIP fine-tuned with supervised learning distinguishes different categories of defects more clearly compared with the one fine-tuned with contrastive learning. This verifies that supervised learning will lead to more discriminative representations and then aggravate the overfitting problem caused by the limited data, while contrastive learning can learn less discriminative

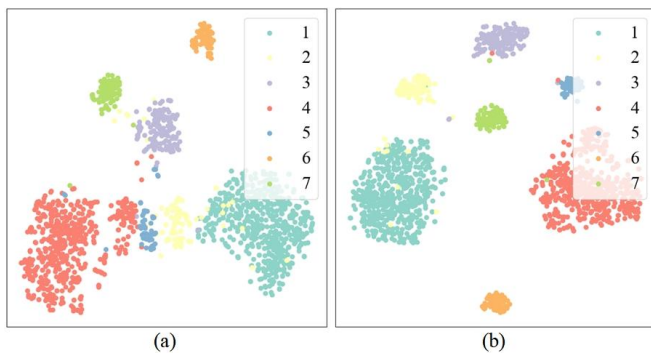


Fig. 10. The t-SNE visualization of 7 categories of defects in the image feature space. (a) CN-CLIP fine-tuned on inspection data with contrastive learning. (b) CN-CLIP fine-tuned on inspection data with supervised learning.

TABLE VII
ABLATION ANALYSIS OF THE FTP STRATEGY

Image Encoder	FTP	TLDC	TLDD
		Acc/%	mAP/%
RN50	-	90.9	75.7
	✓	91.6	76.4
ViT	-	93.3	76.5
	✓	93.8	78.1

* Bold font represents the optimal value.

representations.

Then we fine-tune our models on the TLDC and TLDD datasets to compare the effect of directly fine-tuning the image encoder in an E2E manner and fine-tuning using the FTP strategy, as shown in Table VII. With the introduction of the pre-training objective, the Acc metrics of the fine-tuned classification models with two image encoder architectures are further increased by 0.7% and 0.5%. Meanwhile, the mAP metrics also benefit from the FTP strategy, increasing by 0.7% and 1.6% respectively. This result verifies our assumption that by introducing a contrastive learning objective that tends to learn weakly discriminative representations, the aggravated overfitting problem in the fine-tuning stage can be effectively alleviated. As shown in the solid lines in Fig. 2(b), it can be seen intuitively that when the FTP strategy is used in the fine-tuning stage, the Acc of the model reaches a peak and then remains stable overall while the growth trend of the loss is also significantly suppressed compared with the one of supervised fine-tuning.

V. CONCLUSION

This paper proposes a VLP-based power-specific VFM, namely TL-CLIP, which provides a more dedicated training starting point for downstream transmission line defect recognition tasks. The training of TL-CLIP is divided into two stages. The first stage is power-specific VLP, where we pre-train the model with ITC and two novel auxiliary pre-training tasks specially designed for the scene of transmission line inspection. Among them, CTM helps the model better capture the semantics of different types of components and thus avoid confusion for categories with similar semantics. On the

other hand, DNC makes the model better cognize the abstract concepts about defect and normality so that the model can be more sensitive to defects in the instances. The second stage fine-tunes the model with the pre-training objective, where we use the proposed FTP strategy to fine-tune the pre-trained VFM instead of the traditional supervised fine-tuning. By fine-tuning the VFM with both the supervised learning objective of the downstream task and the contrastive learning objective of ITC, the overfitting problem of the pre-trained VFM during the fine-tuning process is effectively alleviated, which leads to a higher recognition accuracy in the downstream task.

As large-scale multimodal pre-training is receiving widespread attention, this study provides new ideas for the subsequent development of large-scale pre-trained models unique to the power domain. We will further explore the internal relations hidden in the inspection data to provide domain-specific supervision signals for training power-specific VFMs with higher performance. Meanwhile, we will continue to focus on researching more effective fine-tuning strategies to overcome the overfitting problem caused by insufficient data in the power domain. Moreover, we hope to further expand our research to defect recognition tasks in the generation, transmission, transformation, and distribution of power systems, and train more general power-specific VFMs.

REFERENCES

- [1] Y. Lyu, M. Cao, S. Yuan, and L. Xie, "Vision-based plane estimation and following for building inspection with autonomous uav," *IEEE Transactions on Systems, Man, and Cybernetics: Systems*, 2023.
- [2] Z. Zhang, S. Wang, J. Chen, and Y. Han, "A bionic dynamic path planning algorithm of the micro uav based on the fusion of deep neural network optimization/filtering and hawk-eye vision," *IEEE Transactions on Systems, Man, and Cybernetics: Systems*, vol. 53, no. 6, pp. 3728–3740, 2023.
- [3] L. Yang, J. Fan, Y. Liu, E. Li, J. Peng, and Z. Liang, "A review on state-of-the-art power line inspection techniques," *IEEE Transactions on Instrumentation and Measurement*, vol. 69, no. 12, pp. 9350–9365, 2020.
- [4] Z. Wang, Q. Gao, J. Xu, and D. Li, "A review of uav power line inspection," in *Advances in Guidance, Navigation and Control: Proceedings of 2020 International Conference on Guidance, Navigation and Control, ICGNC 2020, Tianjin, China, October 23–25, 2020*. Springer, 2022, pp. 3147–3159.
- [5] Y. Luo, X. Yu, D. Yang, and B. Zhou, "A survey of intelligent transmission line inspection based on unmanned aerial vehicle," *Artificial Intelligence Review*, vol. 56, no. 1, pp. 173–201, 2023.
- [6] D. Sadykova, D. Pernebayeva, M. Bagheri, and A. James, "In-yolo: Real-time detection of outdoor high voltage insulators using uav imaging," *IEEE Transactions on Power Delivery*, vol. 35, no. 3, pp. 1599–1601, 2019.
- [7] Z. Ling, D. Zhang, R. C. Qiu, Z. Jin, Y. Zhang, X. He, and H. Liu, "An accurate and real-time method of self-blast glass insulator location based on faster r-cnn and u-net with aerial images," *CSEE Journal of Power and Energy Systems*, vol. 5, no. 4, pp. 474–482, 2019.
- [8] H. Liang, C. Zuo, and W. Wei, "Detection and evaluation method of transmission line defects based on deep learning," *IEEE Access*, vol. 8, pp. 38 448–38 458, 2020.
- [9] P. Luo, B. Wang, H. Wang, F. Ma, H. Ma, and L. Wang, "An ultrasmall bolt defect detection method for transmission line inspection," *IEEE Transactions on Instrumentation and Measurement*, vol. 72, pp. 1–12, 2023.
- [10] L. Yuan, D. Chen, Y.-L. Chen, N. Codella, X. Dai, J. Gao, H. Hu, X. Huang, B. Li, C. Li *et al.*, "Florence: A new foundation model for computer vision," *arXiv preprint arXiv:2111.11432*, 2021.
- [11] Y. Zhai, X. Yang, Q. Wang, Z. Zhao, and W. Zhao, "Hybrid knowledge r-cnn for transmission line multifitting detection," *IEEE Transactions on Instrumentation and Measurement*, vol. 70, pp. 1–12, 2021.

- [12] Y. Zhai, Q. Wang, X. Yang, Z. Zhao, and W. Zhao, "Multi-fitting detection on transmission line based on cascade reasoning graph network," *IEEE Transactions on Power Delivery*, vol. 37, no. 6, pp. 4858–4868, 2022.
- [13] C. Dong, K. Zhang, Z. Xie, J. Wang, X. Guo, C. Shi, and Y. Xiao, "Transmission line key components and defects detection based on meta-learning," *IEEE Transactions on Instrumentation and Measurement*, 2024.
- [14] L. Liu, J. Zhao, Z. Chen, B. Zhao, and Y. Ji, "A new bolt defect identification method incorporating attention mechanism and wide residual networks," *Sensors*, vol. 22, no. 19, p. 7416, 2022.
- [15] H. Choi, J. P. Yun, B. J. Kim, H. Jang, and S. W. Kim, "Attention-based multimodal image feature fusion module for transmission line detection," *IEEE Transactions on Industrial Informatics*, vol. 18, no. 11, pp. 7686–7695, 2022.
- [16] S. Hao, B. An, X. Ma, X. Sun, T. He, and S. Sun, "Pkamnet: a transmission line insulator parallel-gap fault detection network based on prior knowledge transfer and attention mechanism," *IEEE Transactions on Power Delivery*, vol. 38, no. 5, pp. 3387–3397, 2023.
- [17] J. Wu, J. Zeng, Y. Zhou, Y. Zhang, and Y. Zhang, "Few-shot electrical equipment image recognition method based on an improved two-stage fine-tuning approach," *The Journal of Engineering*, vol. 2023, no. 9, p. e12313, 2023.
- [18] F. Zhuang, Z. Qi, K. Duan, D. Xi, Y. Zhu, H. Zhu, H. Xiong, and Q. He, "A comprehensive survey on transfer learning," *Proceedings of the IEEE*, vol. 109, no. 1, pp. 43–76, 2020.
- [19] J. Deng, W. Dong, R. Socher, L.-J. Li, K. Li, and L. Fei-Fei, "Imagenet: A large-scale hierarchical image database," in *2009 IEEE conference on computer vision and pattern recognition*. Ieee, 2009, pp. 248–255.
- [20] A. Radford, J. W. Kim, C. Hallacy, A. Ramesh, G. Goh, S. Agarwal, G. Sastry, A. Askell, P. Mishkin, J. Clark *et al.*, "Learning transferable visual models from natural language supervision," in *International conference on machine learning*. PMLR, 2021, pp. 8748–8763.
- [21] A. Yang, J. Pan, J. Lin, R. Men, Y. Zhang, J. Zhou, and C. Zhou, "Chinese clip: Contrastive vision-language pretraining in chinese," *arXiv preprint arXiv:2211.01335*, 2022.
- [22] C. Jia, Y. Yang, Y. Xia, Y.-T. Chen, Z. Parekh, H. Pham, Q. Le, Y.-H. Sung, Z. Li, and T. Duerig, "Scaling up visual and vision-language representation learning with noisy text supervision," in *International conference on machine learning*. PMLR, 2021, pp. 4904–4916.
- [23] N. Fei, Z. Lu, Y. Gao, G. Yang, Y. Huo, J. Wen, H. Lu, R. Song, X. Gao, T. Xiang *et al.*, "Towards artificial general intelligence via a multimodal foundation model," *Nature Communications*, vol. 13, no. 1, p. 3094, 2022.
- [24] J. Zhu and G. Pang, "Toward generalist anomaly detection via in-context residual learning with few-shot sample prompts," in *Proceedings of the IEEE/CVF Conference on Computer Vision and Pattern Recognition*, 2024, pp. 17 826–17 836.
- [25] Q. Zhou, G. Pang, Y. Tian, S. He, and J. Chen, "Anomalyclip: Object-agnostic prompt learning for zero-shot anomaly detection," in *The Twelfth International Conference on Learning Representations*, 2024.
- [26] Z. Gu, B. Zhu, G. Zhu, Y. Chen, M. Tang, and J. Wang, "Anomalygpt: Detecting industrial anomalies using large vision-language models," in *Proceedings of the AAAI Conference on Artificial Intelligence*, vol. 38, no. 3, 2024, pp. 1932–1940.
- [27] W. Bao, X. Du, N. Wang, M. Yuan, and X. Yang, "A defect detection method based on bc-yolo for transmission line components in uav remote sensing images," *Remote Sensing*, vol. 14, no. 20, p. 5176, 2022.
- [28] Z. Guo, Y. Tian, and W. Mao, "A robust faster r-cnn model with feature enhancement for rust detection of transmission line fitting," *Sensors*, vol. 22, no. 20, p. 7961, 2022.
- [29] K. Zhang, W. Lou, J. Wang, R. Zhou, X. Guo, Y. Xiao, C. Shi, and Z. Zhao, "Pa-detr: End-to-end visually indistinguishable bolt defects detection method based on transmission line knowledge reasoning," *IEEE Transactions on Instrumentation and Measurement*, vol. 72, pp. 1–14, 2023.
- [30] Y. Li, Y. Xu, W. Sun, Q. Qian, Z. Li, and X. Jiang, "Ecc-rcnn: An efficient and high-accuracy object detection framework for transmission line defect identification," *IET Smart Grid*, vol. 7, no. 1, pp. 28–37, 2024.
- [31] Z. Zhao, X. Lv, Y. Xi, and S. Miao, "Defect detection method for key area guided transmission line components based on knowledge distillation," *Frontiers in Energy Research*, vol. 11, p. 1287024, 2023.
- [32] K. Zhang, Y. Xiao, J. Wang, M. Du, X. Guo, R. Zhou, C. Shi, and Z. Zhao, "Dp-gan: A transmission line bolt defects generation network based on dual discriminator architecture and pseudo-enhancement strategy," *IEEE Transactions on Power Delivery*, 2024.
- [33] K. Zhang, R. Zhou, J. Wang, Y. Xiao, X. Guo, and C. Shi, "Transmission line component defect detection based on uav patrol images: A self-supervised hc-vit method," *IEEE Transactions on Systems, Man, and Cybernetics: Systems*, 2024.
- [34] K. Zhou, J. Yang, C. C. Loy, and Z. Liu, "Learning to prompt for vision-language models," *International Journal of Computer Vision*, vol. 130, no. 9, pp. 2337–2348, 2022.
- [35] X. Wu, F. Zhu, R. Zhao, and H. Li, "Cora: Adapting clip for open-vocabulary detection with region prompting and anchor pre-matching," in *Proceedings of the IEEE/CVF conference on computer vision and pattern recognition*, 2023, pp. 7031–7040.
- [36] M. Barraco, M. Cornia, S. Cascianelli, L. Baraldi, and R. Cucchiara, "The unreasonable effectiveness of clip features for image captioning: an experimental analysis," in *proceedings of the IEEE/CVF conference on computer vision and pattern recognition*, 2022, pp. 4662–4670.
- [37] Z. Wang, Z. Wu, D. Agarwal, and J. Sun, "Medclip: Contrastive learning from unpaired medical images and text," in *Proceedings of the 2022 Conference on Empirical Methods in Natural Language Processing*, 2022, pp. 3876–3887.
- [38] X. Han, L. Yu, X. Zhu, L. Zhang, Y.-Z. Song, and T. Xiang, "Fashionvit: Fashion-focused vision-and-language representation learning," in *European conference on computer vision*. Springer, 2022, pp. 634–651.
- [39] S. Mo, M. Kim, K. Lee, and J. Shin, "S-clip: Semi-supervised vision-language learning using few specialist captions," *Advances in Neural Information Processing Systems*, vol. 36, pp. 61 187–61 212, 2023.
- [40] J. Jeong, Y. Zou, T. Kim, D. Zhang, A. Ravichandran, and O. Dabeer, "Winclip: Zero-/few-shot anomaly classification and segmentation," in *Proceedings of the IEEE/CVF Conference on Computer Vision and Pattern Recognition*, 2023, pp. 19 606–19 616.
- [41] J. Yang, C. Li, P. Zhang, B. Xiao, C. Liu, L. Yuan, and J. Gao, "Unified contrastive learning in image-text-label space," in *Proceedings of the IEEE/CVF Conference on Computer Vision and Pattern Recognition*, 2022, pp. 19 163–19 173.
- [42] S. Ren, K. He, R. Girshick, and J. Sun, "Faster r-cnn: Towards real-time object detection with region proposal networks," *IEEE transactions on pattern analysis and machine intelligence*, vol. 39, no. 6, pp. 1137–1149, 2016.
- [43] Y. Li, H. Mao, R. Girshick, and K. He, "Exploring plain vision transformer backbones for object detection," in *European conference on computer vision*. Springer, 2022, pp. 280–296.
- [44] L. Van der Maaten and G. Hinton, "Visualizing data using t-sne." *Journal of machine learning research*, vol. 9, no. 11, 2008.